PHYSICAL REVIEW B **89**, 241404(R) (2014)

Mapping of strained graphene into one-dimensional Hamiltonians: Quasicrystals and modulated crystals

Gerardo G. Naumis* and Pedro Roman-Taboada

Departamento de Física-Química, Instituto de Física, Universidad Nacional Autónoma de México (UNAM), Apartado Postal 20-364, 01000 México, Distrito Federal, México

(Received 27 March 2014; revised manuscript received 28 May 2014; published 11 June 2014)

The electronic properties of graphene under any arbitrary uniaxial strain field are obtained by an exact mapping of the corresponding tight-binding Hamiltonian into an effective one-dimensional modulated chain. For a periodic modulation, the system displays a rich behavior, including quasicrystals and modulated crystals with a complex spectrum, including gaps and peaks at the Fermi energy and localization transitions. All these features are explained by the incommensurate or commensurate nature of the potential, which leads to a dense filling by diffraction spots of the reciprocal space in the former case. The essential features of strain are made specially clear by analyzing a special momenta that uncouples the model into dimers.

DOI: 10.1103/PhysRevB.89.241404 PACS number(s): 73.22.Pr, 71.23.Ft, 03.65.Vf

Graphene is a two-dimensional (2D) carbon crystal [1]. This atom-thin elastic membrane has amazing physical properties [1–4]. Notably, graphene has the highest known interval of elastic response (up to 20% of the lattice parameter [5]). The tailoring of its electronic properties by controlled mechanic deformation is a field known as "straintronics" [6–9]. Also, graphene seems to be the ideal candidate to replace Si in transistors. However, when graphene grows in top of a substrate with different lattice parameters or structure, strain and corrugation appear [10]. The understanding of how strain affects the graphene's electronic properties is clearly a fundamental issue, still in the process of development [11–17]. How strain affects the electronic spectrum and wave functions? By mapping the limiting case of any uniaxial strain to an effective one-dimensional Hamiltonian, we prove that the answer is unexpectedly rich. As we will see, in certain circumstances strain promotes a quasiperiodic fractal electronic behavior due to the complex self-similar structure of the reciprocal space. Furthermore, it is known that a fractal behavior can be obtained in rotated bilayer graphene under magnetic fields [18–21]. Here we prove that a similar effect can be achieved by strain in single-layer graphene. Such effect should be generated by growing graphene in top of a crystal with a slightly different lattice parameter, as is now technically feasible [20]. As is known, this leads to a periodic strain [10]. Then a quasiperiodic behavior should be obtained when the ratio of lattice parameters becomes incommensurate. Other two-dimensional materials like MoS_2 or $NiSe_2$ are expected to present the same effect [22–24].

Let us start with a zigzag graphene nanoribbon, as shown in Fig. 1, with a uniaxial strain applied in the y direction. Although our methodology can be applied for uniaxial strain in the zigzag or arm chair directions, here we will concentrate only in one kind, since we want to bring out the essential features of the model.

The new positions of the carbon atoms are $\boldsymbol{r}' = \boldsymbol{r} + \boldsymbol{u}(y)$, where $\boldsymbol{r} = (x,y)$ are the unstrained coordinates of the atoms and $\boldsymbol{u}(y) = (0,u(y))$ is the corresponding displacement. The electronic properties of graphene are well described by a one orbital next-nearest neighbor tight-binding Hamiltonian in a honeycomb lattice, given by [4]

$$H = -\sum_{\boldsymbol{r}',n} t_{\boldsymbol{r}',n} c^{\dagger}_{\boldsymbol{r}'} c_{\boldsymbol{r}'+\boldsymbol{\delta}'_n} + \text{H.c.}, \tag{1}$$

where $\boldsymbol{r}'$ runs over all sites of the deformed lattice and $\boldsymbol{\delta}'_n$ are the corresponding vectors that point to the three next nearest neighbors of $\boldsymbol{r}'$. For unstrained graphene, $\boldsymbol{\delta}'_n = \boldsymbol{\delta}_n$, where

$$\boldsymbol{\delta}_1 = \frac{a}{2}(\sqrt{3},1), \quad \boldsymbol{\delta}_2 = \frac{a}{2}(-\sqrt{3},1), \quad \boldsymbol{\delta}_3 = a(0,-1). \tag{2}$$

The operators $c^{\dagger}_{\boldsymbol{r}'}$ and $c_{\boldsymbol{r}'+\boldsymbol{\delta}'_n}$ correspond to creating and annihilating electrons on lattice sites. The hopping integral $t_{\boldsymbol{r}',n}$ depends upon strain, which induces bond length changes that increase or decrease the overlap between wave functions. Such variation with the distance can be calculated from [25,26] $t_{\boldsymbol{r}',n} = t_0 exp[-\beta|\boldsymbol{\delta}'_n|/a - 1)]$, where $\beta \approx 3$, $t_0 \approx 2.7eV$ corresponds to nonstrained pristine graphene, and a is the bond length, which will be taken as $a = 1$ in what follows.

For strain in one direction, we can map exactly the Hamiltonian into an effective one dimensional system as the nanoribbon is made from cells of four nonequivalent atoms [27] with coordinates $\boldsymbol{r}' = (x, y_s'^{(m)})$, where $s = 1,2,3,4$ and m denotes the number of the cell, as sketched out in Fig. 1. For graphene without strain, the positions in the y direction are given by $y_1^{(m)} = 3m$, $y_2^{(m)} = 3m + 1/2$, $y_3^{(m)} = 3m + 3/2$, and $y_4^{(m)} = 3m + 2$. On each of these sites, a strain field $u(y)$ is applied, resulting in new positions $y_s'^{(m)} = y_s^{(m)} + u_s^{(m)}$ where $u_s^{(m)}$ is a short hand notation for $u(y_s^{(m)})$. For uniaxial strain, the symmetry along the nonstrained x direction is not broken. Thus the solution of the Schrödinger equation $H\Psi(\boldsymbol{r}') = E\Psi(\boldsymbol{r}')$ for the energy E has the form $\Psi(\boldsymbol{r}') = \exp(ik_x x)\psi_s(m)$, where k_x is the wave vector in x direction and $\psi_s(m)$ is only a function of $y_s'^{(m)}$, where s and m label the sites along the zigzag path in the vertical direction, as indicted in Fig. 1. Taking into account that for each bond that cross the dotted lines in Fig. 1, we need to add a phase $\exp(\pm ik_x\sqrt{3}/2)$ for the wave function, it is easy

*naumis@fisica.unam.mx

 ©2014 American Physical Society

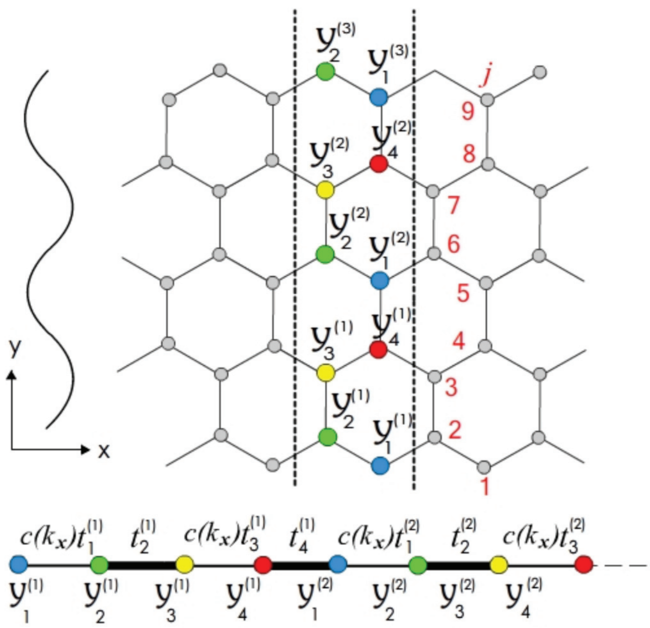

FIG. 1. (Color online) Mapping of zigzag strained graphene into a chain. The directions x and y are defined at the left. The strain in the y direction is sketched out using a wavy curve, while the boundaries of the unitary cell in the x direction are shown with dots. Inside the cell, four kinds of inequivalent sites appear (shown in different colors), denoted by $y_s^{(m)}$. The effective Hamiltonian of the zigzag path in the y direction that joins sites $y_s^{(m)}$ can be mapped into the chain that appears below, where the label j corresponds to the site along the zigzag path as indicated. For the special momenta $k_x = \pi/\sqrt{3}$, the model breaks down into dimers, represented by bold links in the chain.

to obtain the following Schrödinger equation,

$$\begin{aligned}
E\psi_1(m) &= c(k_x)t_1^{(m)}\psi_2(m) + t_4^{(m-1)}\psi_4(m-1),\\
E\psi_2(m) &= t_2^{(m)}\psi_3(m) + c(k_x)t_1^{(m)}\psi_1(m),\\
E\psi_3(m) &= c(k_x)t_3^{(m)}\psi_4(m) + t_2^{(m)}\psi_2(m),\\
E\psi_4(m) &= t_4^{(m)}\psi_1(m+1) + c(k_x)t_3^{(m)}\psi_3(m),
\end{aligned} \tag{3}$$

where $c(k_x) = 2\cos(\sqrt{3}k_x/2)$ and $t_s^{(m)} = t_0 exp[-\beta(u_{s+1}^{(m)} - u_s^{(m)})\delta_{s+1,s}^y]$. Here, $\delta_{s+1,s}^y$ denotes the y components of each of the three vectors $\boldsymbol{\delta}_1, \boldsymbol{\delta}_2, \boldsymbol{\delta}_3$ that join sites with y coordinates $y_s^{(m)}$ and $y_{s+1}^{(m)}$ for unstrained graphene. In this formula, one needs to apply the conditions $y_5^{(m)} = y_1^{(m+1)}$ and $y_0^{(m)} = y_4^{(m-1)}$ at the boundary of each cell. Furthermore, the sequence of $y_s^{(m)}$ can be written as $y(j) = \{3j + [1-(-1)^j/2]\}/4$, where j is an integer that labels the site number along the zigzag path in the y axis, given by $j = 4(m-1)+s$. Finally, one can write a Hamiltonian $H(k_x)$ without any reference to cells of four sites,

$$H(k_x) = \sum_j [t_{2j}c_{2j+1}^\dagger c_{2j} + c(k_x)t_{2j+1}c_{2j+2}^\dagger c_{2j+1}] \tag{4}$$

with $t_{[4(m-1)+s]} = t_s^{(m)}$. This gives

$$t_j = t_0 \exp\left[-\beta\frac{3+(-1)^{j+1}}{4}(u_{j+1}-u_j)\right], \tag{5}$$

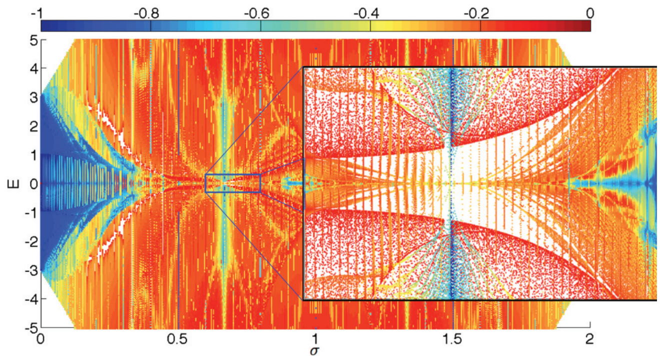

FIG. 2. (Color online) Spectrum as a function of σ for $\lambda = 2$ and $\phi = (4/3)\pi\sigma$ considering the exponential dependence of $t_{r',n}$, obtained by solving the Schrödinger's equation for a system of 200 atoms, using 300 grid points for sampling k_x and with periodic boundary conditions. The inset presents a blow up near zero energy. The different colors represent the localization participation ratio $\alpha(E)$.

where it is understood that u_j is just the displacement of the jth atom along the vertical zigzag path, i.e., $u_j \equiv u_s^{(m)}$. Now $H(k_x)$ describes a chain for any arbitrary uniaxial strain, as indicated in Fig. 1.

The exact mapping can serve as a test for approximate theories of strain in graphene. Consider, for example, an oscillating strain $u(y) = (2/3)(\lambda/\beta)\cos[(8\pi/3)\sigma(y-1/2)+\phi]$ of the type expected when graphene grows on top of a material with a different lattice [10].

Figure 2 shows the complex spectrum of H as a function of σ, revealing a behavior that is akin to the Hofstadter butterfly that appears in the Harper model [28]. The most surprising result is the appearance of gaps around the Femi level $E = 0$ for some values of σ. We can get a better understanding by using a linear approximation for $t_{r',n}$, assuming a small strain as usual in straintronics. Under such approximation, Eq. (5) becomes

$$\frac{t_j}{t_0} = 1 + \lambda\xi(j+1)\sin(\pi\sigma\xi(j))\sin(2\pi\sigma j + \phi), \tag{6}$$

where $\xi(j) = 1 + [(-1)^j/3]$.

The resulting Hamiltonian describes one-dimensional quasicrystals for irrational σ, and modulated crystals for rational σ. Although the model resembles an off-diagonal Harper model [29], there is an important extra modulation provided by $\xi(j+1)\sin(\pi\sigma\xi(j))$. In Fig. 3, we present the resulting bands as a function of k_x and the corresponding density of states (DOS) for $\sigma = 0$ (pure graphene), $3\tau/4$, and $3/4$, where τ is the golden ratio $\tau = (\sqrt{5}-1)/2$. Several interesting features are observed. The first is the disappearance of the Dirac cone for cases (c) and (e), observed around $E = 0$ for pure graphene. In case (c), degenerate states appear at $E = 0$ and the DOS is spiky. On the other hand, in case (f) the DOS is smooth. Only the Van Hove singularities observed for $E = \pm 1$ in pure graphene move and split in two. It is also interesting the behavior of the spectrum as a function of λ for a given σ. In Figs. 4(a) and 4(b), we present the cases $\sigma = 3\tau/4$ and $\sigma = 3/4$. For $\sigma = 3/4$, a gap opens above a certain critical

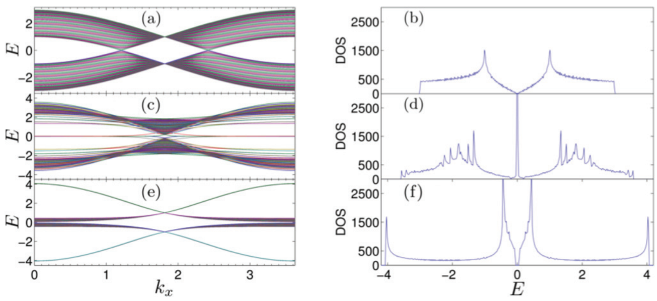

FIG. 3. (Color online) Band structure (left column) and density of states (right column) using $\phi = (4/3)\pi\sigma$ and $\lambda = 2$ for, (a) and (b) unstrained graphene lattice, (c) and (d) strained graphene with $\sigma \approx 3\tau/4$, (e) and (f) strained graphene with $\sigma = 3/4$. Spikes appear for cases (c) and (d), while a gap is seen in (e) and (f) at $E = 0$. Observe in (e) and (f) how the DOS is similar to linear chains perturbed by a small interaction.

λ_C, while for $\sigma = 3\tau/4$, no gaps are seen. Let us explain this rich behavior.

An analysis of Fig. 3(e) suggests that for $\sigma = 3/4$, the behavior is akin to a system of two disconnected chains. Such analysis is confirmed by evaluating Eq. (5) using $\sigma = 3/4$. In this particular case, the strain has the same period as the four site cells, thus $t_s^{(m)}$ turns out to be independent of m, and $t_s^{(m)} = 1 - 4(\lambda/3)\sin(3\pi s/2)$. The corresponding band edges are given by a matrix of 4×4 whose solutions, in terms of the parameters λ and k_x, are $E(\lambda,k_x) = \pm[\sqrt{1 + (8\lambda/9)^2\cos^2(\sqrt{3}k_x/2)} \pm 2\cos(\sqrt{3}k_x/2)]$. A gap opens when $\lambda > \lambda_C = 9\sqrt{3}/8$. For $\lambda = \lambda_M = 9/4$, the system behaves as two disconnected strips of triangular cells, explaining the observed spectrum of Fig. 3(e). The gap (Δ) goes as $\Delta \propto (\lambda - \lambda_C)$ as confirmed by Fig. 4(b).

Figures 3(c) and 4(a) are even more interesting. Here the strain is incommensurate with the four site cell period. The system is thus quasiperiodic. As is well known, perturbation theory can not be used at any order, since the problem is akin to the small divisor problem due to the dense appearance of diffraction peaks in reciprocal space [30]. This fact is important since if a Fourier expansion of the operator $c_{r'}$ is performed as $c_{r'} = \sum_{\boldsymbol{k}} exp[\boldsymbol{k}\cdot(\boldsymbol{r}+\boldsymbol{u}(\boldsymbol{r}))]c_{\boldsymbol{k}}$, where $\boldsymbol{k}$ is a reciprocal vector, then one needs to consider a dense distribution [30,31] in $\sum_{\boldsymbol{k}}\exp[\boldsymbol{k}\cdot\boldsymbol{u}(\boldsymbol{r})]$ for incommensurate cases. This explains the spiky DOS, since for each diffraction spot, a singularity appears [31,32]. To overline this, let us work out a particular example.

For the value $k_x = \pi/\sqrt{3}$, we have that $c(k_x) = 0$. This is valid for any λ or σ. The corresponding Hamiltonian $H(k_x = \pi/\sqrt{3})$ given by Eq. (4) becomes just a model for disconnected dimers, represented in the chain of Fig. 1 as bold lines. The eigenvalues are obtained from an effective 2×2 matrix, from where $E(k_x = \pi/\sqrt{3}) = \pm t_{2l}$, with l an integer. Using Eq. (6), the eigenvalues are $E(k_x = \pi/\sqrt{3}) = \pm[1 + (2/3)\lambda\sin(4\pi\sigma/3)\sin(4\pi\sigma l + \phi)]$. In the case of unstrained graphene, $E(k_x = \pi/\sqrt{3}) = \pm 1$. These two values correspond to the highly degenerate peaks observed in the DOS of Fig. 3(b). Each peak has a degeneracy $N/2$, where N is the number of atoms in the zigzag path. These peaks are associated with a Van Hove singularity, since standing waves due to diffraction appear [31–33]. For $\sigma = 3/4$, $E(k_x = \pi/\sqrt{3}) = \pm 1$. The degeneracy remains, as seen in Fig. 3(e), although it does not produce peaks because all other states are also highly degenerate. However, for irrational σ, the factor $\sin(4\pi\sigma l + \phi)$ behaves as a pseudorandom number generator which fills in a dense way the interval [30] $[-1,1]$. The degeneracy is thus lifted. The spectral type is pure point and contained in the intervals $[-1 - 2\lambda/3, -1 + 2\lambda/3]$ and $[1 - 2\lambda/3, 1 + 2\lambda/3]$, leading to a gap of size $4\lambda/3$ if $\lambda < 3/2$. The splitting is evident at the middle of k_x axis in Fig. 3(c), and when compared with Figs. 3(a) and 3(e). What happens to the wave-function localization? For irrational σ, the eigenfunctions are localized in dimers on the y direction. Obviously, since all $E(k_x = \pi/\sqrt{3})$ are different, an infinite number of reciprocal vectors are needed to generate the corresponding wave functions. Thus, even in this simple case the usual perturbation theory breaks down. However, for rational σ, the eigenvalues are degenerate. Any linear combination of the wave function in dimers is a solution, leading to delocalized states around $k_x = \pi/\sqrt{3}$. Such behavior is revealed by calculating the normalized participation ratio, defined as [34]

$$\alpha(E) = \frac{\ln\sum_{j=1}^{N}|\psi(j)|^4}{\ln N}. \tag{7}$$

The factor $\alpha(E)$ is a measure of localization. In Figs. 2 and 4, the colors indicate the value of $\alpha(E)$. For Fig. 2, a fractal behavior reveals how localization depends on the number theory properties of σ. In Fig. 4(b), the case $\sigma = 3/4$ does not present appreciable changes, as expected from the previous discussion. Only at $\lambda = \lambda_M$ there is a localization transition as a consequence of the breaking into disconnected chains, leading to the vertical red line observed in Fig. 4(b). The case $\sigma = 3\tau/4$ shows the expected localization around $E = \pm 1$ as $\lambda \to \infty$.

Finally, it is worthwhile mentioning how some of the observed effects are related with the zigzag states reported

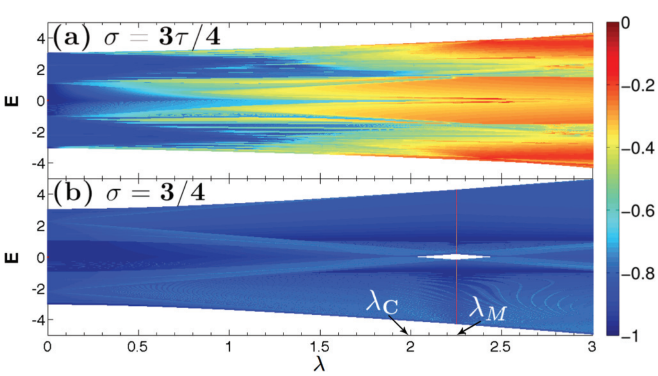

FIG. 4. (Color online) Energy spectrum of graphene under uniaxial sinusoidal strain in the linear approximation as a function of λ for (a) $\sigma = (3\tau/4)$ and (b) $\sigma = 3/4$. In (b), a gap opens for $\lambda > \lambda_C = 9\sqrt{(3)}/8$, while for $\lambda = 9/4$ the system breaks down into disconnected strips of triangular cells. The colors represent the localization participation ratio $\alpha(E)$. Notice the transition at $\lambda = \lambda_M$. The phase was taken as $\phi = (4/3)\pi\sigma$, and periodic boundary conditions were used.

in graphene nanoribbons [35–37] and topological states [38]. In particular, the DOS in the irrational case resembles the case of narrow graphene nanoribbons [35]. The reason for this is simple. For irrational σ, there are sites j in which $t_j \approx 0$, since t_j mimics a random number generator. In such sites, the lattice is almost decoupled in the y direction, producing many effective nanoribbons of different widths. This leads to singularities that are strikingly similar to narrow nanoribbons, as observed inFig. 3(d). In fact, a similar phenomena happens for rational σ and big λ. For example, if $\sigma = 3/4$ and $\lambda = \lambda_D$, t_j is zero at the end of the unitary one dimensional cell and we obtain many effective nanoribbons, but this time all with the same four atom width. In a similar way, the states at the Fermi energy can be explained in many different way: as zigzag states [35] due to an effective decoupling in nanoribbons, as an imbalance in the number of atoms in each bipartite lattice [33] or as strictly confined states [33]. These states have a toplogical nature, as we have verified by changing ϕ and using different boundary conditions.

In conclusion, we have provided an exact mapping into a one dimensional chain for any uniaxial strain in graphene. For a periodic strain, effective quasiperiodic or modulated crystals systems were obtained. Due to the dense nature of the reciprocal space, the spectrum and localization properties presented a fractal pattern. Gaps, singularities, and localized states were observed. These features can not be predicted by simple perturbation theory techniques. The quasiperiodic nature of the problem found here, suggests the paramount importance of disorder due to the intrinsic instability of such spectra [39–42] and the possibility of building equivalent superlattices [43]. In future work, we will study edge states, since they are expected to present a nesting of topological length scales, given by the Chern numbers, within a fractal pattern, as observed in the Harper and Fibonacci models [38].

This work was supported by DGAPA-PAPIIT IN-102513 and by DGTIC-NES center.

[1] K. S. Novoselov, A. K. Geim, S. V. Morozov, D. Jiang, Y. Zhang, S. V. Dubonos, I. V. Grigorieva, and A. A. Firsov, Science **306**, 666 (2004).
[2] A. K. Geim, Science **324**, 1530 (2009).
[3] A. H. Castro Neto, F. Guinea, N. M. R. Peres, K. S. Novoselov, and A. K. Geim, Rev. Mod. Phys. **81**, 109 (2009).
[4] W. Lu, P. Soukiassian, and J. Boeckl, MRS Bulletin **37**, 1119 (2012).
[5] C. Lee, X. Wei, J. W. Kysar, and J. Hone, Science **321**, 385 (2008).
[6] V. M. Pereira, A. H. Castro Neto, and N. M. R. Peres, Phys. Rev. B **80**, 045401 (2009).
[7] V. M. Pereira and A. H. Castro Neto, Phys. Rev. Lett. **103**, 046801 (2009).
[8] F. Guinea, Solid State Commun. **152**, 1437 (2012).
[9] D. Zhan, J. Yan, L. Lai, Z. Ni, L. Liu, and Z. Shen, Adv. Mater. **24**, 4055 (2012).
[10] N. A. Vinogradov, A. A. Zakharov, V. Kocevski, J. Rusz, K. A. Simonov, O. Eriksson, A. Mikkelsen, E. Lundgren, A. S. Vinogradov, N. Mårtensson, and A. B. Preobrajenski, Phys. Rev. Lett. **109**, 026101 (2012).
[11] A. L. Kitt, V. M. Pereira, A. K. Swan, and B. B. Goldberg, Phys. Rev. B **85**, 115432 (2012).
[12] F. de Juan, J. L. Mañes, and M. A. H. Vozmediano, Phys. Rev. B **87**, 165131 (2013).
[13] A. L. Kitt, V. M. Pereira, A. K. Swan, and B. B. Goldberg, Phys. Rev. B **87**, 159909(E) (2013).
[14] J. V. Sloan, A. A. P. Sanjuan, Z. Wang, C. Horvath, and S. Barraza-Lopez, Phys. Rev. B **87**, 155436 (2013).
[15] S. Barraza-Lopez, A. A. P. Sanjuan, Z. Wang, and M. Vanevi, Solid State Commun. **166**, 70 (2013).
[16] M. Oliva-Leyva and G. G. Naumis, Phys. Rev. B **88**, 085430 (2013).
[17] G. Volovik and M. Zubkov, Ann. Phys. **340**, 352 (2014).
[18] A. Luican, G. Li, A. Reina, J. Kong, R. R. Nair, K. S. Novoselov, A. K. Geim, and E. Y. Andrei, Phys. Rev. Lett. **106**, 126802 (2011).
[19] K. S. Novoselov, E. McCann, S. V. Morozov, V. I. Falko, M. I. Katsnelson, U. Zeitler, D. Jiang, F. Schedin, and A. K. Geim, Nat. Phys. **2**, 177 (2006).
[20] L. A. Ponomarenko, R. V. Gorbachev, G. L. Yu, D. C. Elias, R. Jalil, A. A. Patel, A. Mishchenko, A. S. Mayorov, C. R. Woods, J. R. Wallbank, M. Mucha-Kruczynski, B. A. Piot, M. Potemski, I. V. Grigorieva, K. S. Novoselov, F. Guinea, V. I. Falko, and A. K. Geim, Nature (London) **497**, 594 (2013).
[21] J. R. Wallbank, A. A. Patel, M. Mucha-Kruczyński, A. K. Geim, and V. I. Fal'ko, Phys. Rev. B **87**, 245408 (2013).
[22] K. F. Mak, C. Lee, J. Hone, J. Shan, and T. F. Heinz, Phys. Rev. Lett. **105**, 136805 (2010).
[23] C. Ataca, H. ahin, and S. Ciraci, J. Phys. Chem. C **116**, 8983 (2012).
[24] J. A. Reyes-Retana, G. G. Naumis, and F. Cervantes-Sodi, J. Phys. Chem. C **118**, 3295 (2014).
[25] R. M. Ribeiro, V. M. Pereira, N. M. R. Peres, P. R. Briddon, and A. H. C. Neto, New J. Phys. **11**, 115002 (2009).
[26] F. Guinea, M. I. Katnelson, and A. K. Geim, Nat. Phys. **6**, 30 (2010).
[27] A. Cresti, N. Nemec, B. Biel, G. Niebler, F. Triozon, G. Cuniberti, and S. Roche, Nano Research **1**, 361 (2008).
[28] D. R. Hofstadter, Phys. Rev. B **14**, 2239 (1976).
[29] P. G. Harper, Proc. Phys. Soc., London, Sect. A **68**, 874 (1955).
[30] D. DiVincenzo and P. Steinhardt, *Quasicrystals: The State of the Art*, Series on Directions in Condensed Matter Physics (World Scientific, Singapore, 1999).
[31] G. G. Naumis and F. Lpez-Rodrguez, Physica B **403**, 1755 (2008).
[32] C. Kittel, *Introduction to Solid State Physics*, 6th ed. (Wiley, New York, 1986).
[33] J. Barrios-Vargas and G. G. Naumis, Solid State Commun. **162**, 23 (2013).
[34] G. G. Naumis, Phys. Rev. B **76**, 153403 (2007).
[35] K. Nakada, M. Fujita, G. Dresselhaus, and M. S. Dresselhaus, Phys. Rev. B **54**, 17954 (1996).

[36] W. Yao, S. A. Yang, and Q. Niu, Phys. Rev. Lett. **102**, 096801 (2009).

[37] M. Ijäs, M. Ervasti, A. Uppstu, P. Liljeroth, J. van der Lit, I. Swart, and A. Harju, Phys. Rev. B **88**, 075429 (2013).

[38] I. I. Satija and G. G. Naumis, Phys. Rev. B **88**, 054204 (2013).

[39] G. G. Naumis and J. L. Aragón, Phys. Rev. B **54**, 15079 (1996).

[40] G. G. Naumis and J. Aragn, Phys. Lett. A **244**, 133 (1998).

[41] G. G. Naumis, Phys. Rev. B **71**, 144204 (2005).

[42] J. C. López, G. Naumis, and J. L. Aragón, Phys. Rev. B **48**, 12459 (1993).

[43] R. Nava, J. Tagüeña-Martínez, J. A. del Río, and G. G. Naumis, J. Phys.: Condens. Matter **21**, 155901 (2009).